Environmental Science & Technology

pubs.acs.org/est

Article

Environmental Occurrence, Source Identification, and Health Hazards of Ultrashort-Chain PFAS in the Yangtze River Delta

Xinchen Miao, Wei Ma, Yawen Tian, Hao Luo, Yanan Xing, Lu Zhan, Yitao Pan, Nan Sheng,* and Jiayin Dai

Cite This: *Environ. Sci. Technol.* 2025, 59, 25138−25150

Read Online

ACCESS | Metrics & More | Article Recommendations | Supporting Information

ABSTRACT: Ultrashort-chain per- and polyfluoroalkyl substances (USC-PFAS), defined by three or fewer carbon atoms in their backbone, represent an emerging class of environmental contaminants whose prevalence and hazards remain inadequately characterized. This study conducted a comprehensive survey of seven USC-PFAS and 37 other PFAS compounds in aquatic environments within the Integrated Demonstration Zone of the Yangtze River Delta, a region undergoing continued industrialization. Results showed that USC-PFAS overwhelmingly dominated PFAS profiles, with trifluoroacetic acid (TFA) representing the most abundant species. Mean concentrations of TFA reached 8.7 × 10^4 ng/L in surface water, 8.0 × 10^4 ng/L in source water, and 6.9 × 10^4 ng/L in tap water, constituting 90.1% to 99.6% of total $\sum_{44}$PFAS across matrices. When TFA was excluded, the remaining $\sum_{6}$USC-PFAS contributed 44.0% to 58.8% of the total PFAS burden. Trifluoromethanesulfonic acid (TFMS) was the second most abundant in surface and source waters, while trifluoromethane sulfonimide (Ntf2) ranked second in tap water. Source apportionment analyses implicated battery electrolyte formulations as major contributors of TFMS and Ntf2. Hazard prioritization based on persistence, mobility, bioaccumulation, and toxicity (PMBT) metrics, alongside measured environmental levels, identified TFA, TFMS, perfluoro-2-(perfluoromethoxy)propanoic acid (PMPA), and perfluorooctanoic acid (PFOA) as high-hazard compounds. These findings suggest that USC-PFAS constitute a pervasive and underregulated class of pollutants, whose high mobility and recalcitrance challenge current assumptions regarding their environmental safety and call for urgent regulatory reevaluation.

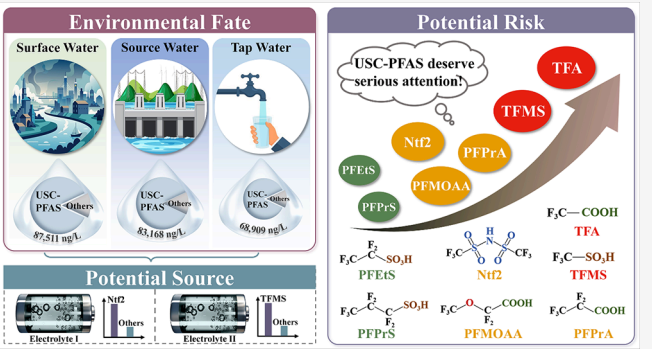

KEYWORDS: *ultrashort-chain PFAS (USC-PFAS), Yangtze River Delta, source apportionment, hazard assessment, TFA, TFMS*

INTRODUCTION

Per- and polyfluoroalkyl substances (PFAS) comprise a structurally varied class of synthetic compounds extensively applied in industrial manufacturing and consumer products due to their superior hydrophobicity,[1] oleophobicity,[2] and thermal stability.[3,4] However, these same properties contribute to their environmental persistence, high mobility, potential for bioaccumulation, and documented toxicity, raising widespread concern over their long-term ecological and health impacts.[5−7] Based on their fluorinated carbon backbone lengths, PFAS can be categorized into ultrashort-chain (USC-PFAS, C1−C3), short-chain (SC-PFAS, C4−C7), and long-chain (LC-PFAS, >C7) subclasses.[8−10] Regulatory attention has primarily focused on long- and short-chain PFAS, including perfluorooctanesulfonic acid (PFOS, C8), perfluorooctanoic acid (PFOA, C8), perfluorohexanesulfonic acid (PFHxS, C6), and perfluorocarboxylic acid (C9−C21), which have been listed under the Stockholm Convention on Persistent Organic Pollutants in 2009, 2019, 2023, and 2025, respectively.[11−14]

In contrast, USC-PFAS has occupied a peripheral position in PFAS research, primarily due to the perception that their shorter carbon chains are associated with reduced toxicity. With the exception of trifluoroacetic acid (TFA), these USC PFAS have received little attention.[15,16] However, this situation is now changing as recent studies have revealed their widespread occurrence in various environmental media at extremely high concentrations. To date, seven USC-PFAS have been detected in environmental matrices: TFA, pentafluoropropionic acid (PFPrA), trifluoromethanesulfonic acid (TFMS), perfluoroethanesulfonic acid (PFEtS), perfluoropropanesulfonic acid (PFPrS), perfluoro-2-methoxyacetic acid (PFMOAA), and bis(trifluoromethyl)amine (Ntf2). Among

Received: July 8, 2025
Revised: November 9, 2025
Accepted: November 10, 2025
Published: November 19, 2025

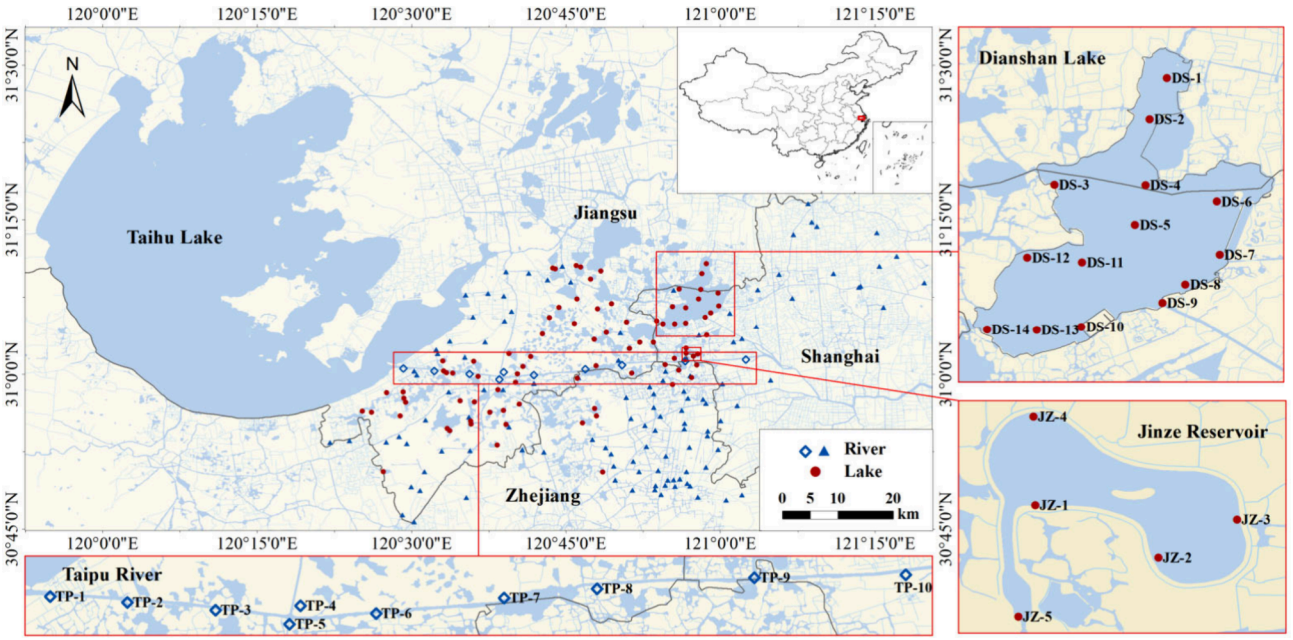

Figure 1. Sampling area and sampling sites in the Shanghai-Zhejiang-Jiangsu junction of the Yangtze River Delta, China. A total of 211 sites were sampled across 67 lakes (red points) and 82 rivers (blue triangles and diamonds). Latitude and longitude are shown at the edge of the main map. Scale and legends are shown in the lower right corner.

these, TFA exhibits the broadest distribution and highest measured concentrations, with levels ranging from 0.01 up to 140 000 ng/L in global surface waters and from 15 to 11017 ng/L in tap and bottled water.[8] TFA has also been detected in the atmosphere, soil, and sediment, highlighting its pervasive presence and capacity for long-range environmental transport.[17]

Compared to TFA, the environmental occurrence of other USC-PFAS remains less well-characterized. Monitoring reveals PFPrA and TFMS occur globally across aquatic systems at ng/L to μg/L concentrations,[18,19] while PFEtS and PFPrS in US groundwater reach extreme concentrations (up to 63 μg/L).[20] PFMOAA has also been reported in estuarine water from the Xiaoqing River in Shandong China, at mean levels of 1 670 ng/L,[21] and demonstrated significant human exposure. Notably, PFMOAA has been detected in 100% of infant urine samples and in 95.5% of human milk samples at concentration of several ng/L,[22] and PFPrA and TFMS have been found at comparable concentrations in maternal cord blood, further demonstrating significant human exposure beginning at early developmental stages.[23] Environmental levels of Ntf2 also display marked geographic variability, with concentrations in Taihu Lake, China, reaching 234.1 ng/L, compared to only 1.9 ng/L in German surface water.[17,19] These disparities reflect both regional differences in PFAS usage and insufficient global surveillance of USC-PFAS. Collectively, these findings demonstrate that USC-PFAS are present at high and continuously rising concentrations globally. Given their high mobility and resistance to degradation, current levels or future accumulation may exceed the safety threshold. These compounds represent a challenge for current environmental monitoring frameworks and regulatory policy.

Preliminary regulatory measures targeting USC-PFAS have been implemented across several European countries. The European Union has established a maximum threshold of 500 ng/L for total PFAS in drinking water, encompassing USC-PFAS.[24] In Denmark, the national parliament has recommended a TFA guideline of less than 9 μg/L in drinking water, while the German Federal Environmental Agency has issued a provisional guideline value of 60 μg/L.[25,26] Although toxicological data on USC-PFAS remain limited, existing experimental evidence has indicated that TFA exposure of rats for 90 days at doses exceeding the no observed adverse effect level (8.4 mg/kg bw/day in males and 10.1 mg/kg bw/day in females) is associated with hematological changes, alterations in clinical chemistry parameters, and increased liver weight.[27] The overall effect of TFA on rat liver is relatively mild, and the adverse effects mentioned above are usually reversible after discontinuation of exposure.[27] Meanwhile PFMOAA exposure (10 mg/kg/d) in juvenile rats has been shown to increase liver weight, reduce thyroid hormone levels, and trigger a series of adverse reactions similar to those observed with PFOA and hexafluoropropylene oxide dimer acid (HFPO-DA).[28,29] Additionally, low-dose TFMS exposure in mice has been linked to hepatic lipid metabolism dysregulation and shifts in gut microbial composition.[30] These data underscore the urgent need for more comprehensive toxicological evaluations to better define the environmental and health implications of USC-PFAS.

The present study assessed PFAS contamination in aquatic environments spanning the Shanghai-Zhejiang-Jiangsu junction of the Yangtze River Delta, a region characterized by rapid industrial development and dense population. The investigation aimed to (1) characterize the spatial and temporal patterns of USC-, SC-, and LC-PFAS in surface water, source water, and tap water; (2) perform source apportionment to identify major contributors of PFAS pollution; and (3) apply a multicriteria hazard-based framework to prioritize PFAS of concern. The results of this study offer critical insights into the environmental distribution, emission sources, and potential hazards associated with USC-PFAS in the Yangtze River Delta region, informing future monitoring and regulatory strategies.

https://doi.org/10.1021/acs.est.5c09274
Environ. Sci. Technol. 2025, 59, 25138−25150

MATERIALS AND METHODS

Sample Collection and Preparation. Water samples: Surface and source water samples were collected in September 2024 (wet season) from 210 sites across 67 lakes and 82 rivers in the Yangtze River Delta region, China (Figure 1 and Table S1) yielding 210 water samples. In March 2025 (dry season), a target subset of 29 sites was resampled, comprising 14 sites in Dianshan Lake (the largest freshwater lake in Shanghai and an alternative water source for the Jinze Reservoir), 10 sites along the Taipu River (a transboundary channel originating from Lake Taihu and a primary water source for the Jinze Reservoir), and five sites in the Jinze Reservoir (one of the four major drinking water sources in Shanghai) providing 29 additional water samples. These 29 dry season sites were all included in the initial wet season campaign (identical GPS coordinates), selected based on their hydrological connectivity, ecological significance, and direct relevance to pathways of exposure to humans via drinking water.[31] Tap water samples were collected from four major drinking water treatment plants (DWTPs) in Shanghai (see Table S2 in the Supporting Information). Additionally, seven commercial electrolyte samples were obtained directly from various electrolyte production facilities. At each sampling location, 1 L of water was collected using a stainless-steel sampler and transferred into polypropylene bottles precleaned with methanol and ultrapure water. Samples were transported on ice to the laboratory and stored at − 20 °C until analysis. Water samples were filtered through glass fiber filters (0.7 μm, 47 mm, Whatman, UK) and extracted using Oasis WAX solid phase extraction (SPE) cartridges (6 cc/150 mg, 30 μm, Waters Corporation, USA).[32] Common carp *(Cyprinus carpio)* (n = 20) were captured from Dianshan Lake during the same September 2024 campaign as surface water (Table S3). Whole blood (1−3 mL) was immediately collected into EDTA-coated vacutainer tubes (BD Biosciences, USA). Muscle, liver, kidney, and gill tissues were dissected and stored at − 80 °C. Biota tissues were extracted from homogenized and diluted samples using methanol following established protocols.[33] Full extraction procedures are provided in the Supporting Information (Text S1).

Targeted Analysis of PFAS. Quantitative determination of PFAS was performed using ultrahigh performance liquid chromatography (UPLC, 1290 Infinity III, Agilent, CA, USA) coupled with triple-quadrupole mass spectrometry (MS, 6495D, Agilent). To capture a broad spectrum of PFAS contamination, the analysis encompassed an extensive suite of target compounds. After excluding analytes with detection frequencies below 50% or mean concentrations below 0.03 ng/L, a total of 44 PFAS were analyzed, including seven USC-PFAS (TFA, PFPrA, TFMS, PFEtS, PFPrS, PFMOAA, Ntf2), 23 SC-PFAS, and 14 LC-PFAS. Quantification was carried out using the internal standard method. In cases where exact internal standards were unavailable, structurally similar analogs were employed for calibration. Detailed descriptions of compound structures, analytical targets, instrumental parameters, and method protocols are provided in Text S2 and Tables S4−S6.

Quality Assurance and Quality Control (QA/QC). Procedural blanks were included in each batch of 10 samples to monitor potential background contamination introduced during extraction. For compounds with persistent trace levels in blanks—PFPrA (0.6 ng/L), PFBA (0.2 ng/L), PFOA (0.8 ng/L), TFMS (0.3 ng/L), and PFBS (0.2 ng/L)—results were corrected by blank subtraction to mitigate matrix effects and improve accuracy. For TFA, which exhibited higher blanks (mean 10.2 ng/L) due to its volatility and trace laboratory environmental ubiquity, corrected concentrations remained analytically robust as blank levels were orders of magnitude lower than sample concentrations. For these compounds, method detection limits (MDLs) were calculated as the mean blank concentration plus three times the standard deviation. For PFAS not detected in blanks, MDLs were defined as the maximum of the lowest calibration level or the concentration corresponding to a signal-to-noise (S/N) ratio of 10.

Quantification was based on internal calibration curves (r^2) exceeding 0.995. Calibration standards were analyzed alongside each batch and loaded prior to each analysis to verify that measured concentrations remained within 20% of the theoretical values. Spike and extraction recoveries for all 44 target PFAS ranged from 80% to 120%, with the exception of TFA, which exhibited a spike recovery of 70.5% and a matrix effect of 74.5%. Additional QA/QC metrics and validation data are presented in Text S3 and Table S7.

Source Apportionment Methods. Source apportionment was performed using a combination of multivariate statistical techniques and receptor modeling approaches. Initial data exploration included principal component analysis (PCA) and factor analysis (FA), both conducted using IBM SPSS Statistics v26 (Chicago, IL, USA). Positive matrix factorization (PMF, v5.0, published by the US EPA) was applied to identify pollutant sources and quantify the contribution of model-driven factors.[34,35] This model decomposes the observed data matrix into factor contributions and source profiles, enabling the identification of distinct source categories and their relative contributions across the data set. Detailed analysis processes are described in Text S4.

Source apportionment fingerprints resolved by the PMF model were integrated with spatial concentration data sets to estimate source-specific contributions at each sampling site. To facilitate cross-site comparisons and reduce the influence of outliers, the resulting values were normalized to a mean of 1. Spatial interpolation was subsequently performed using the inverse distance weighting (IDW) method in ArcGIS to generate continuous concentration heatmaps, allowing the visualization of dominant source hotspots across the study region.

Hazard Prioritization. A multicriteria hazard prioritization framework integrating both exposure and hazard dimensions was employed, following established methodologies.[36,37] Hazard potential (HP) was assessed based on the Persistence, Mobility, Bioaccumulation, and Toxicity (PMBT) attributes of each PFAS. In contrast to previous studies, bioaccumulation potential was assessed using empirically derived biological accumulation factors (BAF) from measured concentrations in fish tissues, with equal weighting applied across all PMBT parameters.[19]

Persistence was characterized using biotransformation half-life values ($t_{1/2}$) in water and fish, as predicted by the graph attention network model.[38] Mobility was assessed using 195 experimental organic carbon−water partition coefficients (Koc) values from Comptox, PubChem and OECD covering 17 PFAS.[39−41] For substances with no measured values available, we use the simulation results from the Graph Attention Network Model as a substitute.[38] Toxicity thresholds were primarily derived from experimental end points from

https://doi.org/10.1021/acs.est.5c09274
Environ. Sci. Technol. 2025, 59, 25138−25150

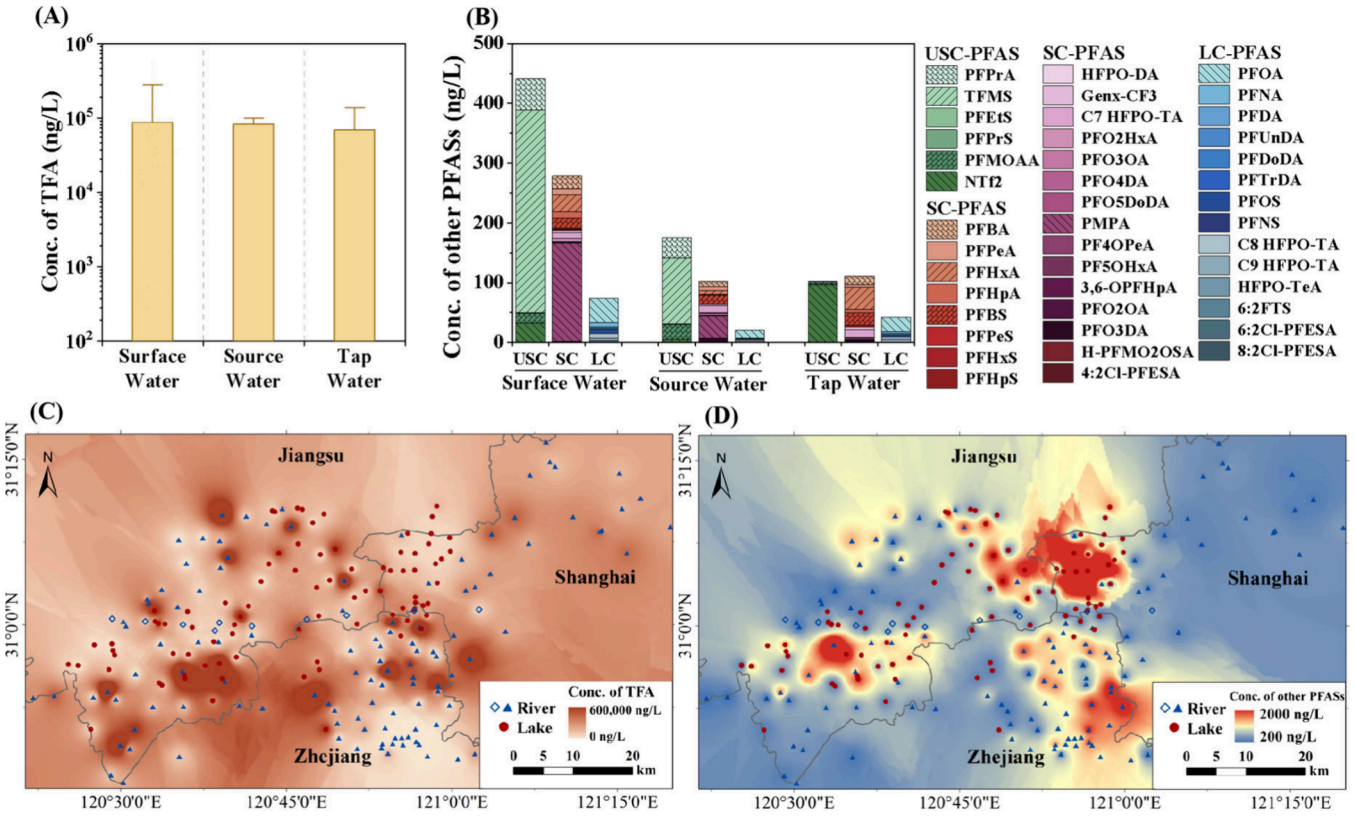

Figure 2. Concentrations and spatial distribution of PFAS in surface, source, and tap water across the Yangtze River Delta. (A) Bar charts showing concentrations of TFA in surface water (n = 206), source water (n = 5), and tap water (n = 4). Error bars represent the standard deviation (SD) of the mean. (B) Stacked bar charts showing concentrations of 43 other PFAS in the same water matrices. Different colors represent different PFAS species: green squares for other USC-PFAS (C1−C3), red squares for SC-PFAS (C4−C7), and blue squares for LC-PFAS (C8 and above). Color gradients from light to dark represent increasing carbon chain lengths and categories from PFCAs, PFSAs, PFECAs to others. (C, D) Geographic heatmap of TFA (C) and (D) concentrations across sampling sites (including surface and source water) by inverse distance weighting. Latitude and longitude are shown at the edge of the main map. Scale bar and legends are shown in the lower right corner.

ECOTOX, Comptox, PubChem and OECD of fish covering 12 PFAS.[39−42] Where experimental data were unavailable, predictions from a AI-based model were used.[43] HP scores were ranked using a toxicological priority index (ToxPi) weighted scoring system[44] (Table S8). PFAS concentrations were subjected to arctangent transformation to mitigate the influence of right-skewed distributions caused by extreme values, followed by min-max normalization to a 0−1 scale.[45] Exposure potential (EP) was calculated as the product of detection frequency (DF) and the normalized concentration. The final hazard index (HI) was derived by multiplying the normalized HP and EP values.[36] HI combines exposure potential and intrinsic hazard, and serves exclusively as a relative ranking method. Detailed analytical processes are described in Text S5.

Based on HI values, PFAS were categorized into four hazard categories: high (HI ≥ 0.1), medium (0.01 ≤ HI < 0.1), low (0.001 ≤ HI < 0.01), and negligible (HI < 0.001).

RESULTS

Distribution and Compositional Profile of PFAS. Across the Yangtze River Delta region, a total of 44, 41, and 34 PFAS were detected in the surface, source, and tap water samples, with 26, 38, and 33 PFAS showing 100% detection frequency, respectively (Figure S1A and S1B). Five USC-PFAS (TFA, TFMS, PFEtS, PFMOAA, and Ntf2) were consistently detected in all surface water samples, while complete detection (100%) of all seven USC-PFAS were observed in source water. In tap water, all USC-PFAS except PFEtS were detected in every sample.

TFA was the most abundant PFAS across water types, with mean concentrations sequentially decreasing from surface water (8.7×10^4 ng/L) to source water (8.3×10^4 ng/L) and tap water (6.89×10^4 ng/L) (Figure 2A). TFA levels exceeded those of all other PFAS by 2−6 orders of magnitude. Concentrations of the remaining 43 PFAS are provided in Figures 2B and S2 and Tables S9−S11. Among USC-PFAS, TFMS ranked second in surface and source water, but third in tap water. PFPrA ranked third in surface and source water. Notably, Ntf2 concentrations in tap water exceeded those in surface and source water, ranking second only to TFA. PFMOAA was detected at concentrations of 16.9, 24.7, and 1.7 ng/L in surface, source, and tap water, respectively.

Among SC-PFAS, PMPA was dominant in surface (165.0 ng/L) and source water (37.1 ng/L) but was not detected in tap water. In contrast, PFHxA showed the highest concentration in tap water (37.2 ng/L), followed by PFBS (20.3 ng/L) and PFBA (13.7 ng/L). C7 HFPO-TA was detected at 9.9 ng/L in surface water, 11.2 ng/L in source water, and 13.6 ng/L in tap water. Among LC-PFAS, PFOA was the most abundant across all water types, with mean concentrations of 40.4, 13.1, and 25.1 ng/L in surface, source, and tap water, respectively. C8 HFPO-TA ranked second in surface water (7.5 ng/L) and tap water (4.5 ng/L), and third in source water

https://doi.org/10.1021/acs.est.5c09274
Environ. Sci. Technol. 2025, 59, 25138−25150

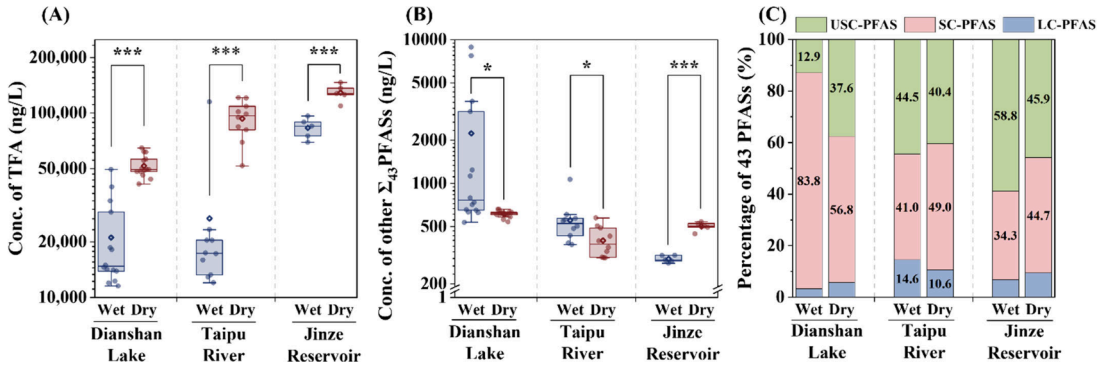

Figure 3. Seasonal variation in PFAS concentrations and compositional profiles in key water bodies of the Yangtze River Delta. (A, B) Seasonal variations in TFA (A) and $\sum_{43}$PFAS (B) concentrations in Dianshan Lake, Taipu River, and Jinze Reservoir. Asterisks represent statistical significance between groups based on *t*-tests (*: $p < 0.05$, **: $p < 0.01$, ***: $p < 0.001$). (C) Seasonal variations in relative composition of PFAS (excluding TFA) in the same areas.

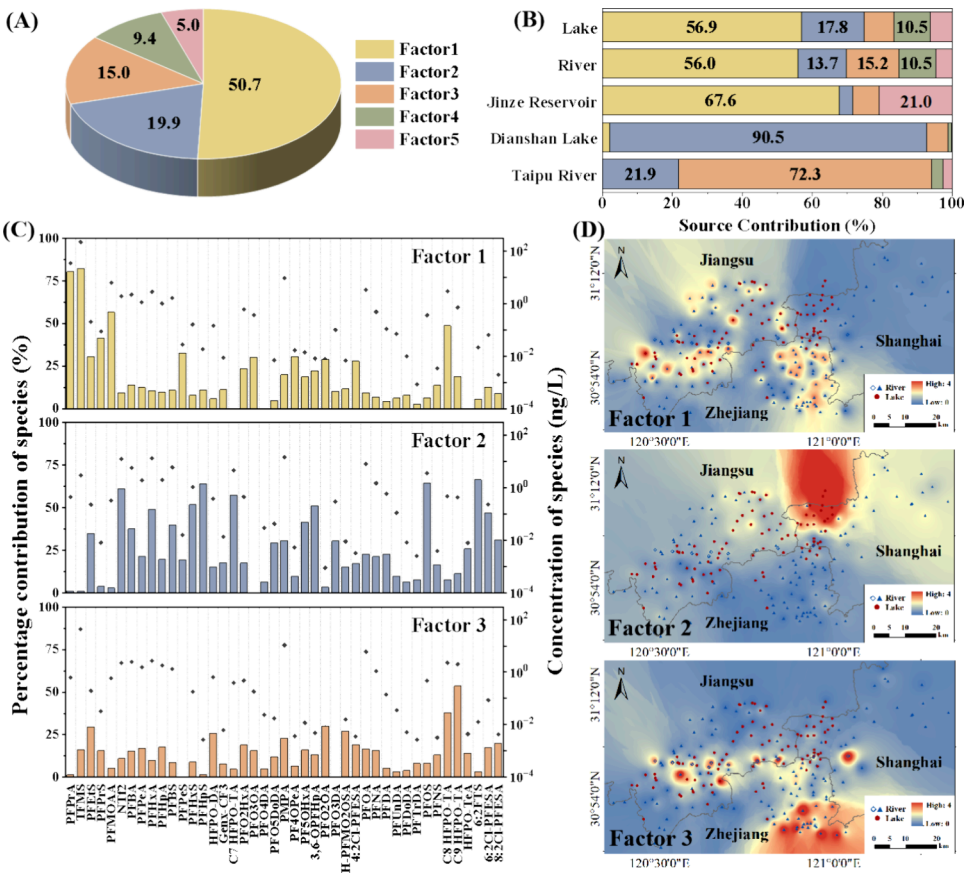

Figure 4. Source apportionment of PFAS in surface and source waters based on PMF modeling. (A) Percentage of source contributions to $\sum_{43}$PFAS concentration. (B) Spatial source contribution profiles at identified stations. Only source factors contributing ≥5% are labeled. Color legend is consistent with (A). (C) Concentration and percentage contributions of individual PFAS to source factors 1−3 derived from PMF model analysis. Different colors represent different factors. Bar heights represent absolute contributions of PFAS (ng/L), and overlaid black dots indicate relative percentage contribution of each PFAS to each factor. (D) Spatial distribution of relative contributions from source factors 1−3 across sampling sites, interpolated using inverse distance weighting. Factors were normalized to a mean of 1. Legends and scales are shown in the lower right corner.

(2.0 ng/L). C9 HFPO-TA ranked second in source water (2.6 ng/L) and third in tap water (4.2 ng/L). PFOS consistently ranked fourth, with concentrations of 6.3, 1.2, and 3.7 ng/L in surface, source, and tap water, respectively.

TFA accounted for 90.1%−99.6% of total $\sum_{44}$PFAS concentrations across all water types. When TFA was excluded, the remaining six USC-PFAS still dominated, contributing 55.6%, 58.8%, and 40.0% of $\sum_{43}$PFAS in surface, source, and tap water, respectively. $\sum_{23}$SC-PFAS contributed 35.1%, 34.3%, and 43.3%, while $\sum_{14}$LC-PFAS contributed 9.4%, 6.9%, and 16.7% in the corresponding matrices.

Spatial distribution analysis revealed pronounced heterogeneity in PFAS concentrations. Heatmaps of TFA showed the highest levels in the Ditang River (R57) (Figure 2C). Total

https://doi.org/10.1021/acs.est.5c09274
Environ. Sci. Technol. 2025, 59, 25138−25150

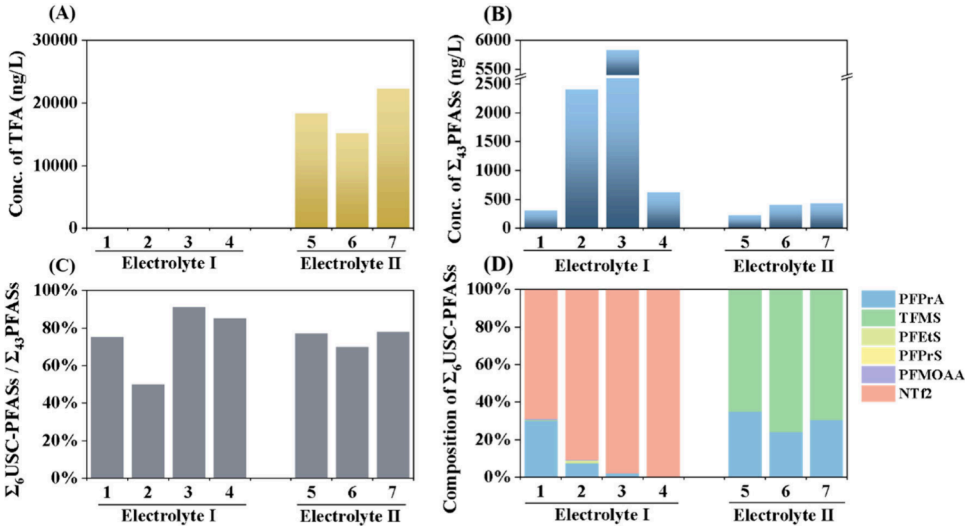

Figure 5. Concentrations and compositional profiles of USC-PFAS in industrial electrolyte samples. (A) Concentration of TFA in electrolyte samples. (B) Concentration of $\sum_{43}$PFAS in electrolyte samples. (C) Percentage of $\sum_{6}$USC-PFAS relative to $\sum_{43}$PFAS in electrolyte samples. (D) Compositional profiles of $\sum_{6}$USC-PFAS in electrolyte samples.

concentrations of the other 43 PFAS ranged from 202.4 to 8 871.6 ng/L, showing hotspots concentrated in Dianshan Lake (L66, western Shanghai), the Ditang River (R57, southeastern Jiangsu), and the Hongqitang/Luxutang Rivers (R42−R45, northeastern Zhejiang) (Figure 2D). In contrast, sampling sites in Shanghai (R2−R29, L1−L19) exhibited relatively low $\sum_{44}$PFAS levels. While $\sum_{23}$SC-PFAS and $\sum_{14}$LC-PFAS demonstrated minimal regional variation except at a few isolated sites, $\sum_{6}$USC-PFAS exhibited pronounced spatial heterogeneity with substantial concentration fluctuations (Figures S2B and S2C).

Seasonal Variation in Surface Water. Marked seasonal differences in concentrations of PFAS were observed between the wet and dry seasons across surface water bodies (Figures 3A, 3B, and S3A). Concentrations of TFA were consistently higher in the dry season in Dianshan Lake, Taipu River, and Jinze Reservoir. Conversely, concentrations of $\sum_{43}$PFAS exhibited more variable patterns, with higher levels during the wet season in Dianshan Lake and Taipu River but elevated concentrations in the dry season in Jinze Reservoir.

Seasonal shifts in PFAS compositional profiles were also evident (Figures 3C and S3B−E). In Dianshan Lake, the contribution of USC-PFAS to $\sum_{43}$PFAS increased substantially in the dry season, driven primarily by an increase in TFMS from 1.7% in the wet season to 24.0% in the dry season. Conversely, SC-PFAS dominated in the wet season, with PMPA accounting for 73.0% of $\sum_{43}$PFAS. In the Taipu River and Jinze Reservoir, however, the relative abundance of $\sum_{6}$USC-PFAS declined in the dry season due to a reduction in TFMS contribution. This shift coincided with an increased proportion of $\sum_{23}$SC-PFAS, attributable to elevated contributions of PFHxA and C7 HFPO-TA, despite a concurrent decline in PMPA levels.

Source Apportionment of PFAS. Five factors were resolved based on FA-PMF model analysis, identifying and quantifying potential PFAS sources in surface and source water across the Yangtze River Delta (Figure S4). Notably, TFA alone accounted for 97.8% of total explained variance due to its extreme abundance, which disproportionately skewed the model and suppressed the influence of other compounds. As a result, TFA was excluded from subsequent source apportionment analyses of the remaining 43 PFAS to ensure meaningful interpretation of source contributions.

The five-factor solution explained 50.7%, 19.9%, 15.0%, 9.4%, and 5.0% of the total variance in $\sum_{43}$PFAS, respectively (Figure 4A). Source profiles varied markedly across key water bodies, with Dianshan Lake, Taipu River, and Jinze Reservoir exhibiting distinct patterns compared to other sites in the region (Figure 4B).

Factor 1 was dominated by USC-PFAS (Figure 4C) and accounted for the majority of TFMS (82.5%), PFPrA (80.5%), and PFMOAA (56.6%), representing the principal source of contamination in the Jinze Reservoir, where it contributed 72.3% of $\sum_{43}$PFAS (Figure 4B). Factor 2 was characterized by elevated 6:2 FTS (66.5%), PFOS (64.4%), PFHpS (64.3%), Ntf2 (61.2%), and C7 HFPO-TrA (57.4%), with strong influence in Dianshan Lake (91%) and neighboring catchments (Figures 4B and 4D). Factor 3 was associated with C9 HFPO-TA (53.6%) and C8 HFPO-TA (37.9%), forming the dominant source in the Taipu River (72.3%) and adjacent zones along the Zhejiang-Shanghai boundary (Figures 4B and 4D). Factor 4 reflected contributions from legacy long-chain perfluorocarboxylic acids (PFCA), including PFUnDA (75.0%), PFDA (63.1%), PFDoDA (62.5%), and PFNA (52.0%), with spatially concentrated impacts in northern Zhejiang (Figures S5A and S5B). Factor 5 was indicative of emerging perfluoroether carboxylic acid (PFECA) sources, such as PFO4DA (88.6%), PFO3DA (59.3%), and GenX-CF3 (49.6%), and displayed relatively uniform distribution across the region (Figure S5A and S5B).

USC-PFAS in Electrolytes. USC-PFAS contamination was evaluated in seven electrolyte samples collected from different manufacturers. Distinct compositional variations emerged, enabling classification of the samples into two clusters (Electrolyte I and II) based on their USC-PFAS signatures. TFA was detected exclusively in Electrolyte II, with concentrations ranging from 1.5×10^4 to 2.2×10^4 ng/L, while remaining below detection limits in all Electrolyte I samples (Figure 5A). Total concentrations of the remaining 43 PFAS (excluding TFA) varied from 176.0 to 5 298.0 ng/L

https://doi.org/10.1021/acs.est.5c09274
Environ. Sci. Technol. 2025, 59, 25138−25150

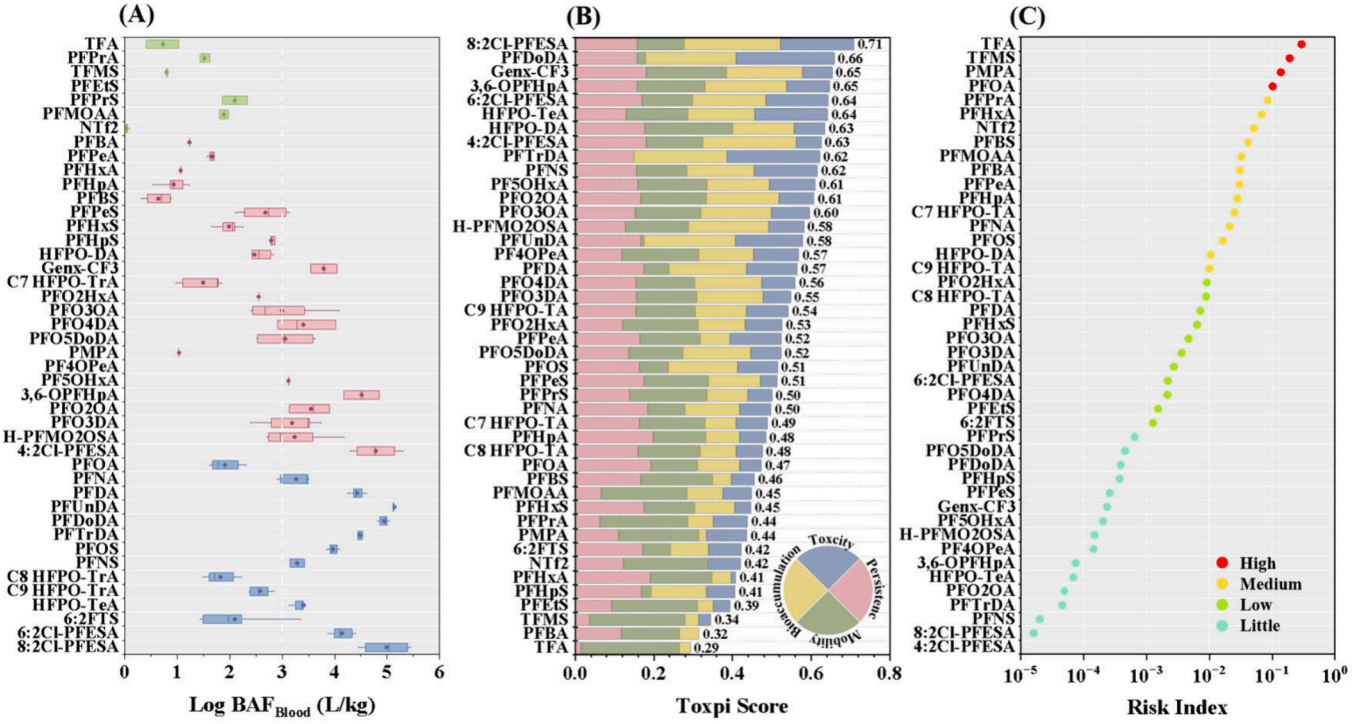

Figure 6. Bioaccumulation, toxicological prioritization, and risk ranking of PFAS. (A) Log-transformed bioaccumulation factors (log BCF) of PFAS in muscle of common carp (*Cyprinus carpio*). Colors represent different types of PFAS. Boxes represent the interquartile range (25th to 75th percentile), with horizontal lines and dots representing median and mean, respectively. (B) ToxPi score rankings for individual PFAS. Scoring criteria are provided in the lower right corner. (C) Risk index rankings of PFAS detected in water samples.

across all samples (Figure 5B). Notably, USC-PFAS were consistently dominant across the data set, accounting for 74.6% to 90.9% of $\sum_{43}$PFAS in all electrolyte samples except Sample 2 (49.6%) (Figure 5C). The two electrolyte groups exhibited distinct molecular fingerprints: Ntf2 was the predominant compound in Electrolyte I, whereas TFMS was the principal constituent in Electrolyte II (Figure 5D).

Bioaccumulation Factors (BAF) of PFAS in Tissues from Common Carp. PFAS concentrations were quantified in five tissue types—blood, gill, kidney, liver, and muscle—collected from Dianshan Lake (Table S12). Across all tissues, 44 PFAS compounds were detected, including 43 in blood, 42 in muscle, and 41 in the gills, kidney, and liver. Detection frequencies ranged from 4.0% to 100.0%, with 32 compounds present in more than 50% of the samples. $\sum_{44}$PFAS concentrations across tissues ranged from 78.8 to 672.5 ng/g w.w. Blood exhibited significantly higher PFAS accumulation than all other tissues ($p < 0.001$, Table S13), with a mean concentration of 542.9 ng/g w.w., dominated by LC-PFAS, which accounted for 71.4% of the total burden. In contrast, $\sum_{44}$PFAS levels in gill, kidney, liver, and muscle ranged from 157.4 to 248.0 ng/g w.w., with $\sum_{7}$USC-PFAS contributing 31.9% to 50.2% of the total, the vast majority of which (95.6%−98.4%) was attributable to TFA (Figure S6A).

BAFs were calculated for all five tissue types to evaluate compound-specific accumulation potential (Figures 6A and S6B−E). Due to its consistently high detection frequency and concentration, blood was used as the reference tissue for log-transformed BAF analysis (log BAF_{blood}), providing enhanced resolution of intercompound differences. Among PFAS classes, USC-PFAS exhibited the lowest bioaccumulation potential, with log $BAF_{average}$ values ranging from 0.02 to 2.10, SC-PFAS showed intermediate accumulation, while LC-PFAS displayed the highest average log BAF values. Notably, 10 PFAS exceeded the BAF threshold of 5 000 (log BAF > 3.70), indicating strong bioaccumulation potential. The highest accumulation was observed for 8:2 chlorinated perfluoroalkyl ether sulfonic acid (8:2 Cl-PFESA), with an average log BAF of 4.75.

Hazard-Based Prioritization of PFAS. A comprehensive hazard-based prioritization was conducted for the 44 PFAS detected in surface and source waters across the Yangtze River Delta. Following normalization of exposure levels (Figure S7), TFA exhibited the highest exposure potential, followed by TFMS, PMPA, PFPrA, PFOA, Ntf2, PFHxA, PFBA, PFBS, and PFMOAA, all of which showed normalized exposure values exceeding 0.1.

To address the limitations of conventional single-indicator assessments, a multidimensional ToxPi was calculated for each compound by integrating four key hazard attributes: persistence (P), mobility (M), bioaccumulation (B), and toxicity (T) (Figure 6B and Table S8). LC-PFAS generally exhibited the highest ToxPi scores, followed by SC-PFAS, while USC-PFAS received the lowest ToxPi scores. Although TFA and TFMS displayed negligible persistence and minimal ecotoxicity among the assessed compounds, both compounds ranked first and second in terms of mobility, underscoring their potential for widespread environmental dissemination and raising concern.

Four compounds (TFA, TFMS, PMPA, and PFOA) were classified as high-hazard (HI > 0.1), while 13 compounds were categorized as medium-hazard (0.01 < HI < 0.1), including three USC-PFAS (PFPrA, Ntf2, and PFMOAA) (Figure 6C).

https://doi.org/10.1021/acs.est.5c09274
Environ. Sci. Technol. 2025, 59, 25138−25150

DISCUSSION

USC-PFAS have long been overlooked in environmental PFAS research.[8,15,20] However, mounting evidence has revealed pervasive environmental distribution and rising concentrations.[8,46] signaling a potential shift in contamination profiles where USC-PFAS may eclipse LC-PFAS as primary contaminants of concern. Despite this emerging threat, the sources, environmental behavior, and health risks of these contaminants, such as TFA, remain inadequately understood. These critical knowledge gaps require reevaluation of their environmental fate, emission pathways, and ecological impact.

The total PFAS concentrations measured in this study markedly exceeded those previously reported for surface waters in the Yangtze River Delta between 2011 and 2022.[35−37] Critically, even after excluding USC-PFAS to align with earlier analytical scopes, legacy SC/LC-PFAS levels have increased by 1.2−6.8 times compared to historical baselines over the past 15 years, demonstrating a consistent upward trajectory (Table S14),[47−51] reflecting their persistent accumulation. Nevertheless, the USC-PFAS accounted for up to 99.6% of $\sum_{44}$PFAS burden, with SC-PFAS and LC-PFAS contributing only 0.3% and 0.1%, respectively, indicating a profound compositional shift in the understanding of regional PFAS pollution.

TFA, the most abundant USC-PFAS, exemplifies this trend in freshwater systems. Globally, surface water concentrations of TFA in freshwater bodies have risen sharply, from approximately 100 ng/L in the 1990s to 1 400 ng/L by 2010—equating to an estimated annual increase of 19%.[8] Present-day TFA levels in freshwater across Europe, North America, Asia, and Oceania typically range from 140 to 260 ng/L, significantly surpassing concentrations observed in Africa (31 ng/L) and South America (12 ng/L) (Table S15).[8,17,52−54] In the current study, mean TFA concentrations in surface waters of the Yangtze River Delta were approximately 62-fold higher than the global reference level from 2010, highlighting the severity of regional contamination. Moreover, TFA levels exceeded those of all other PFAS by 1−5 orders of magnitude, establishing it as the dominant contributor to total PFAS burden of the region.

Other USC-PFAS demonstrated pronounced enrichment across the Yangtze River Delta compared to reported global surface water concentrations. While previous studies have reported median TFMS levels of 30 ng/L in Sweden,[52] 8.0 ng/L in Germany,[20] and 5 ng/L in the USA (Table S15),[8,53] median concentrations in this study reached 117.9 ng/L, exceeding those in the upper Yangtze River Basin (53.5 ng/L)[55] by 2.2-fold. Similarly, PFPrA was detected at 51.8 ng/L, surpassing the global baseline of 1.9 ng/L.[8] Notably, Ntf2 demonstrated a regional concentration of 19.6 ng/L, comparable to levels recorded in Taihu Lake (21.7 ng/L)[19] and exceeding those in German waters (0.8 ng/L) by 23-fold,[20] establishing it as a regional marker of USC-PFAS contamination.

Furthermore, PFAS levels in surface waters of the Yangtze River Delta exhibited distinct seasonal variations, with an interesting inverse trend observed for TFA compared to other PFAS. TFA concentrations rose during dry seasons as reduced precipitation diminished the effects of dilution, contrasting with wet-season declines from dilution by rainfall. Interestingly, $\sum_{43}$PFAS levels in Dianshan Lake and Taipu River were higher during the wet season. This anomaly reflects enhanced atmospheric deposition where precipitation removes particle-bound PFAS,[56,57] coupled with elevated humidity accelerating atmospheric oxidation of volatile precursors like FTOHs.[58,59] Concurrently, increased riverine runoff in Taipu River amplified upstream inputs. The proportional contribution of USC-PFAS was higher during wet seasons, driven by storm runoff mobilizing diffuse sources. Conversely, dry seasons amplified the relative abundance of SC-PFAS via the Yin-Jiang-Ji-Tai Project, which engineered transfer channeled industrial signatures, specifically C7 HFPO-TA and PFHxA, from upstream fluorochemical clusters into Taihu Lake, propagating through Taipu River to accumulate in Jinze Reservoir.[19,47] Dianshan Lake initially deviated from this pattern due to an exceptional wet-season influx of PMPA, which may come from a point-source pollutant. This convergence with Taihu Lake and Jinze Reservoir confirms that intrinsic PFAS partitioning is uniformly governed by hydro-climatic forces, with point sources acting as localized overrides.

TFA exhibited exceptionally high concentrations with a remarkably uniform spatial distribution across the entire study area, which prevented the identification of distinct point sources in the present study. Generally, the exponential escalation of TFA concentrations is largely driven by the atmospheric degradation of fluorinated precursors, particularly refrigerants.[8,54] Hydrofluorocarbons (HFCs), which account for over half of global production, most of which occurs in China, are being phased out and progressively replaced by hydrofluoroolefins (HFOs) as part of international regulatory efforts.[60−63] One widely adopted replacement, hydrofluoroolefin-1234yf (HFO-1234yf), is manufactured in the upstream fluorochemical manufacturing zone of the present study area. With a short atmospheric lifetime of approximately 12 days, HFO-1234yf is almost entirely transformed into TFA via rapid atmospheric oxidation.[64,65] The resulting TFA is subsequently deposited into terrestrial and aquatic environments through both wet and dry atmospheric deposition processes,[65,66] leading to spatially concentrated TFA accumulation near emission sources.[60] In parallel, C−CF3 moieties present in fluorinated agrochemicals, pharmaceuticals, and industrial polymers exhibit strong recalcitrance to enzymatic and photolytic degradation. While partial incorporation into nonextractable residues (NER) occurs, these structures can undergo terminal fragmentation to mineralize into TFA.[54,67,68] Given the high degree of industrialization, dense population, and intensive chemical manufacturing in the Yangtze River Delta region, these combined emission pathways likely explain the markedly elevated TFA concentrations detected in local aquatic environments.

Among these detected USC-PFAS, TFMS, PFPrA, and PFMOAA exhibited common-source features, implicating precursor degradation of SC- and LC-PFAS in aquatic systems throughout the Yangtze River Basin.[8] Their high mobility likely facilitates rapid downstream transport and dispersion through interconnected waterways across the Yangtze River Delta region.[59] In addition to transformation pathways, direct emissions from upstream fluorochemical manufacturing zones—among the largest in China—serve as substantial contributors. TFMS, with global annual production of 100−1 000 tons, is primarily synthesized for use as an industrial catalyst.[20,69] Its lithium salt form (LiTFMS), used in electrolyte formulations for lithium-ion batteries,[70] represents a probable but unquantified source. PFPrA is formed through atmospheric degradation of fire protection fluids[71,72] and thermal decomposition of fluoropolymers used in coatings,

https://doi.org/10.1021/acs.est.5c09274
Environ. Sci. Technol. 2025, 59, 25138−25150

cookware, and combustion engines.[73] Ntf2 emerged as a regional fingerprint contaminant with distinct source features. Commercially produced as lithium bis-(trifluoromethanesulfonyl)imide (LiTFSI) by the 3 M company, this compound is a widely used additive in battery electrolytes, antistatic agents, and polyvinylidene fluoride (PVDF)-based electrode and separator materials. Continuous release throughout production, application, and disposal phases within local battery industrial parks likely drives its environmental presence.[20,70,74] These findings underscore the dual contribution of precursor transformation and direct industrial emissions in shaping the environmental behavior and dominance of USC-PFAS in the Yangtze River Delta.

Although industrial literature identifies both TFMS and Ntf2 as common lithium battery electrolyte additives, source apportionment revealed distinct environmental source profiles for the two compounds. Seven industrial electrolyte samples were analyzed in this study, which were subsequently classified into two distinct compositional categories. Class I electrolytes were characterized by high Ntf2 concentrations, consistent with its established use in lithium-ion battery systems.[74] In contrast, Class II electrolytes exhibited TFMS as the dominant component, indicating that the electrolyte manufacturing sector may serve as an unrecognized emission source of TFMS. This compound may be introduced into the environment through operational pathways such as charge−discharge processes during electrode reactions, though direct emission pathways remain unverified due to inaccessibility of effluent data. Further research is needed to provide more direct evidence. This compositional divergence observed across samples provides direct molecular evidence linking electrolyte production to the environmental release of USC-PFAS, particularly Ntf2 and TFMS. A substantial number of electrolyte manufacturing facilities are distributed throughout the Yangtze River Delta (Table S16), underscoring the regional relevance of this emission pathway. Potential sources of environmental contamination include leakage during electrolyte manufacturing, improper disposal of spent battery electrolytes, and uncontrolled release of synthetic intermediates or byproducts during large-scale production. These findings highlight a need for further investigation into the contributions of the electrolyte industry to USC-PFAS burdens in surrounding ecosystems.

Following the transfer of surface water into the reservoir system, pretreatment processes, including aeration, sodium hypochlorite disinfection, and activated carbon adsorption, led to an initial reduction in PFAS concentrations relative to untreated surface water. Subsequent treatment by DWTPs further decreased PFAS levels, with notable efficiency observed for TFMS, the concentration of which declined from 110.8 ± 7.0 ng/L in source water to 2.8 ± 0.4 ng/L in tap water, corresponding to a removal efficiency of 97.5%. Despite this, tap water remained heavily contaminated by TFA, which reached a mean concentration of 6.88×10^4 ng/L, 3 orders of magnitude higher than the next most abundant compound, Ntf2. Although no national regulatory limits for TFA in drinking water currently exist in China, concentrations of TFA in all samples exceeded the health-based guidance value of 9 μg/L proposed by the Danish Parliament, and half of the samples surpassed the 60 μg/L threshold set by the German Federal Environment Agency (Umweltbundesamt, UBA) (Figure S8).[8] Notably, Ntf2 emerged as the second most prevalent PFAS in tap water, exhibiting 8−28-fold increases compared to its source water concentrations. To the best of our knowledge, this represents the first report of the dominance of Ntf2 in a municipal drinking water supply. Moreover, the concentration of Ntf2 was significantly higher in tap water than in source water. This enrichment is hypothesized to result from several mechanisms: chlorine-induced cleavage of sulfonamide precursors, potential microbial dealkylation in the distribution system, and point-source contamination from industries like electroplating. However, direct mechanistic evidence remains limited and requires further validation. Similarly, C7 HFPO-TA demonstrated a progressive increase in concentration from surface water to source water to tap water. The elevation in tap water might be attributed to water treatment processes and leaching from pipeline materials, while the higher level in the source water is linked to the inflow from Dianshan Lake, which carries elevated concentrations of C7 HFPO-TA.

The high concentrations of Ntf2 pose substantial concerns for potential ecological and human health impacts, especially given the current lack of comprehensive toxicological data. The ToxPi framework enabled a comprehensive assessment of PFAS hazard potential across multiple dimensions.[44] For SC- or LC-PFAS, persistence, bioaccumulation, and ecotoxicity were identified as core hazard drivers, each exhibiting strong positive correlations with increasing fluorinated chain length.[75] In contrast, BAFs for USC-PFAS ranged from 1.02 to 480.00, remaining well below the US EPA threshold for bioaccumulative substances (BAF $\geq$ 1 000), indicating low biological retention. Despite limited bioaccumulation, these compounds exhibited extremely high environmental mobility, a property that facilitates long-distance dispersal through aquatic systems.[67,76] This mobility is particularly consequential in the Yangtze River Delta, where downstream hydrology and a dense, interconnected water network promote extensive redistribution across ecological boundaries. Although TFA exhibited lower ecotoxicity, persistence, and bioaccumulation potential than PFOA, its exceptional mobility and environmental abundance resulted in a higher composite HI score, identifying it as a compound with relative high hazard in Yangtze River Delta. TFMS, which has been reported to disrupt lipid metabolism, alters gut microbial composition in mice,[30] and inhibits growth in *in vitro* assays,[77] also ranked as a relatively high-hazard compound, and surpassed its long-chain homologue PFOS. PFPrA, PFMOAA and Ntf2, were categorized as medium hazard compounds with high aqueous concentrations and pronounced mobility as their hazard drive, which mirrored that of TFA and TFMS. These findings collectively underscore the emerging environmental significance of USC-PFAS and challenge existing prioritization frameworks that focus predominantly on long-chain compounds.

■ ENVIRONMENTAL IMPLICATIONS

This study provides the first comprehensive evidence that USC-PFAS can infiltrate municipal water supply systems via industrial discharge, pinpointing electrolyte manufacturing as a previously unrecognized but significant emission source of Ntf2, TFMS, and PFPrA. The elevated concentrations of USC-PFAS in aquatic environments, particularly TFA and TFMS, coupled with emerging ecotoxicological evidence, challenge the long-held assumption of their low-hazard profile.[8,54] TFA, TFMS, PFPrA, Ntf2, and PFMOAA surpass legacy prioritized compounds such as PFOS and/or PFOA in overall environ-

https://doi.org/10.1021/acs.est.5c09274
Environ. Sci. Technol. 2025, 59, 25138−25150

mental hazard ranking within the Yangtze River Delta. It should be emphasized that the HI applied in this study serves as a preliminary screening tool for identifying priority compounds under data-limited conditions. Furthermore, the equal-weighting scheme within the PMBT framework represents a screening-level simplification that may overemphasize long-term potential hazards (persistence and mobility) while underestimating biological impacts (bioaccumulation and toxicity). This approach might introduce assessment bias for substances with disproportionate hazard drivers. A comprehensive environmental risk assessment will require further substance-specific toxicological and exposure evaluations. Despite their widespread distribution and increasing prominence, USC-PFAS remain largely absent from current regulatory frameworks. Given the limited existing understanding of their environmental fate, source traceability, toxicokinetics, and health implications, targeted research into USC-PFAS source attribution, environmental transformation, and biological effects is urgently needed. In the context of rapid industrialization and urbanization, the continued focus on LC-PFAS may leave critical exposure pathways unaddressed. These findings underscore the urgent need to enhance environmental health surveillance systems, implement stricter emission control strategies, and revise existing regulations to accommodate the growing threat posed by USC-PFAS.

■ ASSOCIATED CONTENT

Supporting Information

The Supporting Information is available free of charge at https://pubs.acs.org/doi/10.1021/acs.est.5c09274.

Details on sample preparation, standards and reagents, quality control and assurance, source apportionment methods, hazard prioritization of PFAS, sampling locations, tap water treatment processes, common carp information, PFAS structures, instrumental parameters, method detection limits (MDL) and recovery rates, ToxPi criteria, variance analysis in fish tissues, electrolyte-related industry information, PFAS concentrations in surface water, source water, tap water, and collected fish, USC-PFAS from previous studies, PFAS detection status, seasonal variations, principal component analysis (PCA) of 44 PFAS, bioaccumulation factors (BAFs) of fish, environmental persistence (EP) rankings, and the ratio of PFAS concentrations in tap water to guideline values (PDF)

Additional tables of concentrations (XLSX)

■ AUTHOR INFORMATION

Corresponding Author

Nan Sheng − *State Key Laboratory of Green Papermaking and Resource Recycling, Key Laboratory of Environmental Health Impact Assessment of Emerging Contaminants, Ministry of Ecology and Environment, School of Environmental Science and Engineering, Shanghai Jiao Tong University, Shanghai 200240, China;* orcid.org/0000-0002-6075-4934; Email: shengnan@sjtu.edu.cn

Authors

Xinchen Miao − *State Key Laboratory of Green Papermaking and Resource Recycling, Key Laboratory of Environmental Health Impact Assessment of Emerging Contaminants, Ministry of Ecology and Environment, School of Environmental Science and Engineering, Shanghai Jiao Tong University, Shanghai 200240, China*

Wei Ma − *State Key Laboratory of Green Papermaking and Resource Recycling, Key Laboratory of Environmental Health Impact Assessment of Emerging Contaminants, Ministry of Ecology and Environment, School of Environmental Science and Engineering, Shanghai Jiao Tong University, Shanghai 200240, China*

Yawen Tian − *State Key Laboratory of Green Papermaking and Resource Recycling, Key Laboratory of Environmental Health Impact Assessment of Emerging Contaminants, Ministry of Ecology and Environment, School of Environmental Science and Engineering, Shanghai Jiao Tong University, Shanghai 200240, China*

Hao Luo − *State Key Laboratory of Green Papermaking and Resource Recycling, Key Laboratory of Environmental Health Impact Assessment of Emerging Contaminants, Ministry of Ecology and Environment, School of Environmental Science and Engineering, Shanghai Jiao Tong University, Shanghai 200240, China*

Yanan Xing − *State Key Laboratory of Green Papermaking and Resource Recycling, Key Laboratory of Environmental Health Impact Assessment of Emerging Contaminants, Ministry of Ecology and Environment, School of Environmental Science and Engineering, Shanghai Jiao Tong University, Shanghai 200240, China; Shanghai Academy of Environmental Sciences, Shanghai 200233, China*

Lu Zhan − *State Key Laboratory of Green Papermaking and Resource Recycling, Key Laboratory of Environmental Health Impact Assessment of Emerging Contaminants, Ministry of Ecology and Environment, School of Environmental Science and Engineering, Shanghai Jiao Tong University, Shanghai 200240, China;* orcid.org/0000-0002-2988-1302

Yitao Pan − *State Key Laboratory of Green Papermaking and Resource Recycling, Key Laboratory of Environmental Health Impact Assessment of Emerging Contaminants, Ministry of Ecology and Environment, School of Environmental Science and Engineering, Shanghai Jiao Tong University, Shanghai 200240, China;* orcid.org/0000-0001-6496-8174

Jiayin Dai − *State Key Laboratory of Green Papermaking and Resource Recycling, Key Laboratory of Environmental Health Impact Assessment of Emerging Contaminants, Ministry of Ecology and Environment, School of Environmental Science and Engineering, Shanghai Jiao Tong University, Shanghai 200240, China;* orcid.org/0000-0003-4908-5597

Complete contact information is available at: https://pubs.acs.org/10.1021/acs.est.5c09274

Notes

The authors declare no competing financial interest.

■ ACKNOWLEDGMENTS

This work was supported by the National Natural Science Foundation of China (W2511014, U22A20618, 2276122, and 2276124).

■ REFERENCES

(1) Park, M.; Wu, S.; Lopez, I. J.; Chang, J. Y.; Karanfil, T.; Snyder, S. A. Adsorption of Perfluoroalkyl Substances (PFAS) in Groundwater by Granular Activated Carbons: Roles of Hydrophobicity of PFAS and Carbon Characteristics. *Water Res.* **2020**, *170*, No. 115364.

(2) Dhore, R.; Murthy, G. S. Per/Polyfluoroalkyl Substances Production, Applications and Environmental Impacts. *Bioresour. Technol.* **2021**, *341*, No. 125808.
(3) Evich, M. G.; Davis, M. J. B.; McCord, J. P.; Acrey, B.; Awkerman, J. A.; Knappe, D. R. U.; Lindstrom, A. B.; Speth, T. F.; Tebes-Stevens, C.; Strynar, M. J.; Wang, Z.; Weber, E. J.; Henderson, W. M.; Washington, J. W. Per- and Polyfluoroalkyl Substances in the Environment. *Science* **2022**, *375* (6580), No. eabg9065.
(4) Mifkovic, M.; Van Hoomissen, D. J.; Vyas, S. Conformational Distributions of Helical Perfluoroalkyl Substances and Impacts on Stability. *J. Comput. Chem.* **2022**, *43* (24), 1656−1661.
(5) Costello, E.; Rock, S.; Stratakis, N.; Eckel, S. P.; Walker, D. I.; Valvi, D.; Cserbik, D.; Jenkins, T.; Xanthakos, S. A.; Kohli, R.; Sisley, S.; Vasiliou, V.; La Merrill, M. A.; Rosen, H.; Conti, D. V.; McConnell, R.; Chatzi, L. Exposure to Per- and Polyfluoroalkyl Substances and Markers of Liver Injury: A Systematic Review and Meta-Analysis. *Environ. Health Perspect.* **2022**, *130* (4), No. 046001.
(6) Zarębska, M.; Bajkacz, S.; Hordyjewicz-Baran, Z. Assessment of Legacy and Emerging PFAS in the Oder River: Occurrence, Distribution, and Sources. *Environ. Res.* **2024**, *251*, No. 118608.
(7) Zhan, W.; Qiu, W.; Ao, Y.; Zhou, W.; Sun, Y.; Zhao, H.; Zhang, J. Environmental Exposure to Emerging Alternatives of Per- and Polyfluoroalkyl Substances and Polycystic Ovarian Syndrome in Women Diagnosed with Infertility: A Mixture Analysis. *Environ. Health Perspect.* **2023**, *131* (5), No. 057001.
(8) Zhi, Y.; Lu, X.; Munoz, G.; Yeung, L. W. Y.; De Silva, A. O.; Hao, S.; He, H.; Jia, Y.; Higgins, C. P.; Zhang, C. Environmental Occurrence and Biotic Concentrations of Ultrashort-Chain Perfluoroalkyl Acids: Overlooked Global Organofluorine Contaminants. *Environ. Sci. Technol.* **2024**, *58* (49), 21393−21410.
(9) Ateia, M.; Maroli, A.; Tharayil, N.; Karanfil, T. The Overlooked Short- and Ultrashort-Chain Poly- and Perfluorinated Substances: A Review. *Chemosphere* **2019**, *220*, 866−882.
(10) Wang, Q.; Ruan, Y.; Jin, L.; Tao, L. S. R.; Lai, H.; Li, G.; Yeung, L. W. Y.; Leung, K. M. Y.; Lam, P. K. S. Legacy and Emerging Per- and Polyfluoroalkyl Substances in a Subtropical Marine Food Web: Suspect Screening, Isomer Profile, and Identification of Analytical Interference. *Environ. Sci. Technol.* **2023**, *57* (22), 8355−8364.
(11) Stockholm Convention. Governments Unite to Step-up Reduction on Global DDT Reliance and Add Nine New Chemicals under International Treaty, 2009. Http://Chm.Pops.Int/Convention/Pressrelease/Cop4geneva9may2009/Tabid/542/Languages/En-Us/Default (accessed 2025-11-18).
(12) Stockholm Convention. The New POPs under the Stockholm Convention, 2020. Http://Www.Pops.Int/Theconvention/Thepops/Thenewpops/Tabid/2511/Default (accessed 2025-11-18).
(13) Stockholm Convention. The New POPs under the Stockholm Convention, 2023. Https://Www.Pops.Int/Theconvention/Thepops/Thenewpops (accessed 2025-11-18).
(14) Stockholm Convention. The New POPs under the Stockholm Convention, 2025. Https://Www.Pops.Int/Theconvention/Thepops/Thenewpops (accessed 2025-11-18).
(15) Ateia, M.; Maroli, A.; Tharayil, N.; Karanfil, T. The Overlooked Short- and Ultrashort-Chain Poly- and Perfluorinated Substances: A Review. *Chemosphere* **2019**, *220*, 866−882.
(16) Zahn, D.; Neuwald, I. J.; Knepper, T. P. Analysis of Mobile Chemicals in the Aquatic Environment—Current Capabilities, Limitations and Future Perspectives. *Anal. Bioanal. Chem.* **2020**, *412* (20), 4763−4784.
(17) Neuwald, I. J.; Hübner, D.; Wiegand, H. L.; Valkov, V.; Borchers, U.; Nödler, K.; Scheurer, M.; Hale, S. E.; Arp, H. P. H.; Zahn, D. Ultra-Short-Chain PFASs in the Sources of German Drinking Water: Prevalent, Overlooked, Difficult to Remove, and Unregulated. *Environ. Sci. Technol.* **2022**, *56* (10), 6380−6390.
(18) Jiao, E.; Larsson, P.; Wang, Q.; Zhu, Z.; Yin, D.; Kärrman, A.; van Hees, P.; Karlsson, P.; Qiu, Y.; Yeung, L. W. Y. Further Insight into Extractable (Organo)Fluorine Mass Balance Analysis of Tap Water from Shanghai, China. *Environ. Sci. Technol.* **2023**, *57* (38), 14330−14339.
(19) Fu, Y.; Ji, Y.; Tian, Y.; Zhang, F.; Sheng, N.; Dai, J.; Pan, Y. Unveiling Priority Emerging PFAS in Taihu Lake Using Integrated Nontarget Screening, Target Analysis, and Risk Characterization. *Environ. Sci. Technol.* **2024**, *58* (42), 18980−18991.
(20) Barzen-Hanson, K.; Field, J. Discovery and Implications of C2 and C3 Perfluoroalkyl Sulfonates in Aqueous Film-Forming Foams and Groundwater. *Environ. Sci. Technol. Lett.* **2015**, *2* (4), 95−99.
(21) Li, Y.; Yao, J.; Zhang, J.; Pan, Y.; Dai, J.; Ji, C.; Tang, J. First Report on the Bioaccumulation and Trophic Transfer of Perfluoroalkyl Ether Carboxylic Acids in Estuarine Food Web. *Environ. Sci. Technol.* **2022**, *56* (10), 6046−6055.
(22) Yao, J.; Dong, Z.; Jiang, L.; Pan, Y.; Zhao, M.; Bai, X.; Dai, J. Emerging and Legacy Perfluoroalkyl Substances in Breastfed Chinese Infants: Renal Clearance, Body Burden, and Implications. *Environ. Health Perspect.* **2023**, *131* (3), No. 037003.
(23) Xia, X.; Zheng, Y.; Tang, X.; Zhao, N.; Wang, B.; Lin, H.; Lin, Y. Nontarget Identification of Novel Per- and Polyfluoroalkyl Substances in Cord Blood Samples. *Environ. Sci. Technol.* **2022**, *56* (23), 17061−17069.
(24) European Union. Directive (EU) 2020/2184 of the European Parliament and of the Council of 16 December 2020 on the Quality of Water Intended for Human Consumption, 2020. https://eur-lex.europa.eu/legal-content/EN/TXT/PDF/?uri=CELEX:32020L2184 (accessed 2025-11-18).
(25) Danish Environmental Protection Agency. Stricter Requirements for per- and Polyfluoroalkyl Substances (PFAS), 2020. https://www.retsinformation.dk/eli/lta/2024/940 (accessed 2025-11-18).
(26) Umweltbundesamt. Reducing the Input of Chemicals into Waters: Trifluoroacetate (TFA) as a Persistent and Mobile Substance with Many Sources, 2021. https://www.umweltbundesamt.de/en/publikationen/reducing-the-input-of-chemicals-into-waters (accessed 2025-11-18).
(27) Dekant, W.; Dekant, R. Mammalian Toxicity of Trifluoroacetate and Assessment of Human Health Risks Due to Environmental Exposures. *Arch. Toxicol.* **2023**, *97* (4), 1069−1077.
(28) Conley, J. M.; Lambright, C. S.; Evans, N.; Bangma, J.; Ford, J.; Hill, D.; Medlock-Kakaley, E.; Gray, L. E., Jr. Maternal and Neonatal Effects of Maternal Oral Exposure to Perfluoro-2-Methoxyacetic Acid (PFMOAA) during Pregnancy and Early Lactation in the Sprague−Dawley Rat. *Environ. Sci. Technol.* **2024**, *58* (2), 1064−1075.
(29) Xu, P.; Nian, M.; Xiang, J.; Zhang, X.; Cheng, P.; Xu, D.; Chen, Y.; Wang, X.; Chen, Z.; Lou, X.; Fang, M. Emerging PFAS Exposure Is More Potent in Altering Childhood Lipid Levels Mediated by Mitochondrial DNA Copy Number. *Environ. Sci. Technol.* **2025**, *59* (5), 2484−2493.
(30) Zhou, J.; Shu, R.; Yu, C.; Xiong, Z.; Xiao, Q.; Li, Z.; Xie, X.; Fu, Z. Exposure to Low Concentration of Trifluoromethanesulfonic Acid Induces the Disorders of Liver Lipid Metabolism and Gut Microbiota in Mice. *Chemosphere* **2020**, *258*, No. 127255.
(31) Liu, X.; Wang, X.; Lu, F.; Liu, S.; Chen, K. Evaluation of the Governance Efficiency of Water Environmental Governance Efficiency in Yangtze River Delta from the Perspective of Multivariate Synergies. *Int. J. Environ. Res. Public Health* **2022**, *19* (4), 2347.
(32) Taniyasu, S.; Kannan, K.; So, M. K.; Gulkowska, A.; Sinclair, E.; Okazawa, T.; Yamashita, N. Analysis of Fluorotelomer Alcohols, Fluorotelomer Acids, and Short- and Long-Chain Perfluorinated Acids in Water and Biota. *J. Chromatogr. A* **2005**, *1093* (1), 89−97.
(33) Hansen, K. J.; Clemen, L. A.; Ellefson, M. E.; Johnson, H. O. Compound-Specific, Quantitative Characterization of Organic Fluorochemicals in Biological Matrices. *Environ. Sci. Technol.* **2001**, *35* (4), 766−770.
(34) Meng, L.; Lu, Y.; Wang, Y.; Ma, X.; Li, J.; Lv, J.; Wang, Y.; Jiang, G. Occurrence, Temporal Variation (2010−2018), Distribution, and Source Appointment of Per- and Polyfluoroalkyl Substances (PFAS) in Mollusks from the Bohai Sea, China. *ACS EST Water* **2022**, *2* (1), 195−205.
(35) Zeng, J.; Liu, K.; Liu, X.; Tang, Z.; Wang, X.; Fu, R.; Lin, X.; Liu, N.; Qiu, J. Driving Factor, Source Identification, and Health Risk

of PFAS Contamination in Groundwater Based on the Self-Organizing Map. *Water Res.* **2024**, *267*, No. 122458.
(36) Hu, J.; Lyu, Y.; Chen, H.; Cai, L.; Li, J.; Cao, X.; Sun, W. Integration of Target, Suspect, and Nontarget Screening with Risk Modeling for per- and Polyfluoroalkyl Substances Prioritization in Surface Waters. *Water Res.* **2023**, *233*, No. 119735.
(37) Zhang, X.; Bowman, D. T.; Diamond, M. L.; Helm, P.; Jobst, K. J.; Hao, C.; Kleywegt, S.; Zhang, Z.-F.; Marvin, C.; Zhang, X. Contribution of Coal Tar Sources to Polycyclic Aromatic Compounds and Associated Ecological Risk in Lake Ontario Sediments: Inference from a Novel Marker. *Environ. Sci. Technol.* **2025**, *59* (6), 3193−3204.
(38) Wang, H.; Liu, W.; Chen, J.; Wang, Z. Applicability Domains Based on Molecular Graph Contrastive Learning Enable Graph Attention Network Models to Accurately Predict 15 Environmental End Points. *Environ. Sci. Technol.* **2023**, *57* (44), 16906−16917.
(39) The Organisation for Economic Co-operation and Development. https://www.oecd.org/en.html (accessed 2025-11-18).
(40) PubChem. https://pubchem.ncbi.nlm.nih.gov/ (accessed 2025-11-18).
(41) CompTox Chemicals Dashboard. https://comptox.epa.gov/dashboard/ (accessed 2025-11-18).
(42) ECOTOX. https://cfpub.epa.gov/ecotox/search.cfm (accessed 2025-11-18).
(43) Gustavsson, M.; Käll, S.; Svedberg, P.; Inda-Diaz, J. S.; Molander, S.; Coria, J.; Backhaus, T.; Kristiansson, E. Transformers Enable Accurate Prediction of Acute and Chronic Chemical Toxicity in Aquatic Organisms. *Sci. Adv.* **2024**, *10* (10), No. eadk6669.
(44) Marvel, S. W.; To, K.; Grimm, F. A.; Wright, F. A.; Rusyn, I.; Reif, D. M. ToxPi Graphical User Interface 2.0: Dynamic Exploration, Visualization, and Sharing of Integrated Data Models. *BMC Bioinformatics* **2018**, *19* (1), 80.
(45) Nie, L.; Wang, H.; Xu, Y. Application of the Arctangent Function Model in the Prediction of Ground Mining Subsidence Deformation: A Case Study from Fushun City, Liaoning Province, China. *Bull. Eng. Geol Environ* **2017**, *76* (4), 1383−1398.
(46) U.S. EPA, U.S. Environmental Protection Agency. https://www.epa.gov/home.
(47) Yao, J.; Sheng, N.; Guo, Y.; Yeung, L. W. Y.; Dai, J.; Pan, Y. Nontargeted Identification and Temporal Trends of Per- and Polyfluoroalkyl Substances in a Fluorochemical Industrial Zone and Adjacent Taihu Lake. *Environ. Sci. Technol.* **2022**, *56* (12), 7986−7996.
(48) Liu, J.; Zhao, Z.; Li, J.; Hua, X.; Zhang, B.; Tang, C.; An, X.; Lin, T. Emerging and Legacy Perfluoroalkyl and Polyfluoroalkyl Substances (PFAS) in Surface Water around Three International Airports in China. *Chemosphere* **2023**, *344*, No. 140360.
(49) Cheng, H.; Jin, H.; Lu, B.; Lv, C.; Ji, Y.; Zhang, H.; Fan, R.; Zhao, N. Emerging Poly- and Perfluoroalkyl Substances in Water and Sediment from Qiantang River-Hangzhou Bay. *Sci. Total Environ.* **2023**, *875*, No. 162687.
(50) Yang, L.; Zhu, L.; Liu, Z. Occurrence and Partition of Perfluorinated Compounds in Water and Sediment from Liao River and Taihu Lake, China. *Chemosphere* **2011**, *83* (6), 806−814.
(51) Chen, M.; Wang, Q.; Shan, G.; Zhu, L.; Yang, L.; Liu, M. Occurrence, Partitioning and Bioaccumulation of Emerging and Legacy per- and Polyfluoroalkyl Substances in Taihu Lake, China. *Sci. Total Environ.* **2018**, *634*, 251−259.
(52) Björnsdotter, M. K.; Yeung, L. W. Y.; Kärrman, A.; Jogsten, I. E. Ultra-Short-Chain Perfluoroalkyl Acids Including Trifluoromethane Sulfonic Acid in Water Connected to Known and Suspected Point Sources in Sweden. *Environ. Sci. Technol.* **2019**, *53* (19), 11093−11101.
(53) Jacob, P.; Helbling, D. E. Rapid and Simultaneous Quantification of Short- and Ultrashort-Chain Perfluoroalkyl Substances in Water and Wastewater. *ACS EST Water* **2023**, *3* (1), 118−128.
(54) Arp, H. P. H.; Gredelj, A.; Glüge, J.; Scheringer, M.; Cousins, I. T. The Global Threat from the Irreversible Accumulation of Trifluoroacetic Acid (TFA). *Environ. Sci. Technol.* **2024**, *58* (45), 19925−19935.
(55) Sun, W.; Fu, Z.; Liu, Y.; Bai, Y.; Zhao, Y.; Wang, C.; Wu, F. Per- and Poly-Fluoroalkyl Substances, and Organophosphate Flame Retardants in the Upper Yangtze River: Occurrence, Spatiotemporal Distribution, and Risk Assessment. *Toxics* **2025**, *13* (2), 116.
(56) Björnsdotter, M. K.; Yeung, L. W. Y.; Kärrman, A.; Jogsten, I. E. Mass Balance of Perfluoroalkyl Acids, Including Trifluoroacetic Acid, in a Freshwater Lake. *Environ. Sci. Technol.* **2022**, *56* (1), 251−259.
(57) Li, X.; Wang, Y.; Cui, J.; Shi, Y.; Cai, Y. Occurrence and Fate of Per- and Polyfluoroalkyl Substances (PFAS) in Atmosphere: Size-Dependent Gas-Particle Partitioning, Precipitation Scavenging, and Amplification. *Environ. Sci. Technol.* **2024**, *58* (21), 9283−9291.
(58) Wang, Q.; Ruan, Y.; Lin, H.; Lam, P. K. S. Review on Perfluoroalkyl and Polyfluoroalkyl Substances (PFASs) in the Chinese Atmospheric Environment. *Sci. Total Environ.* **2020**, *737*, No. 139804.
(59) Arp, H. P. H.; Hale, S. E. Assessing the Persistence and Mobility of Organic Substances to Protect Freshwater Resources. *ACS Environ. Au* **2022**, *2* (6), 482−509.
(60) Wang, Y.; Liu, L.; Qiao, X.; Sun, M.; Guo, J.; Zhang, J.; Zhao, B. Projections of National-Gridded Emissions of Hydrofluoroolefins (HFOs) in China. *Environ. Sci. Technol.* **2023**, *57* (23), 8650−8659.
(61) Wu, J.; Martin, J. W.; Zhai, Z.; Lu, K.; Li, L.; Fang, X.; Jin, H.; Hu, J.; Zhang, J. Airborne Trifluoroacetic Acid and Its Fraction from the Degradation of HFC-134a in Beijing, China. *Environ. Sci. Technol.* **2014**, *48* (7), 3675−3681.
(62) Wu, J.; Wang, T.; An, M.; Ding, S.; Yao, B.; Western, L. M.; Purohit, P.; Liu, Z.; Zhang, Z.; Peng, L. Development and Validation of a Gridded Emissions Inventory for HFC-134a in China. *Environ. Int.* **2025**, *200*, No. 109535.
(63) Environmental Effects Assessment Panel (EEAP). https://ozone.unep.org/science/assessment/eeap (accessed 2025-11-18).
(64) Luecken, D. J.; Waterland, R. L.; Papasavva, S.; Taddonio, K. N.; Hutzell, W. T.; Rugh, J. P.; Andersen, S. O. Ozone and TFA Impacts in North America from Degradation of 2,3,3,3-Tetrafluoropropene (HFO-1234yf), A Potential Greenhouse Gas Replacement. *Environ. Sci. Technol.* **2010**, *44* (1), 343−348.
(65) Wang, Y.; Liu, L.; Qiao, X.; Sun, M.; Guo, J.; Zhao, B.; Zhang, J. Atmospheric Fate and Impacts of HFO-1234yf from Mobile Air Conditioners in East Asia. *Sci. Total Environ.* **2024**, *916*, No. 170137.
(66) Wang, Q.; Wang, X.; Ding, X. Rainwater Trifluoroacetic Acid (TFA) in Guangzhou, South China: Levels, Wet Deposition Fluxes and Source Implication. *Sci. Total Environ.* **2014**, *468−469*, 272−279.
(67) Scheurer, M.; Nödler, K.; Freeling, F.; Janda, J.; Happel, O.; Riegel, M.; Müller, U.; Storck, F. R.; Fleig, M.; Lange, F. T.; Brunsch, A.; Brauch, H.-J. Small, Mobile, Persistent: Trifluoroacetate in the Water Cycle − Overlooked Sources, Pathways, and Consequences for Drinking Water Supply. *Water Res.* **2017**, *126*, 460−471.
(68) Cui, J.; Guo, J.; Zhai, Z.; Zhang, J. The Contribution of Fluoropolymer Thermolysis to Trifluoroacetic Acid (TFA) in Environmental Media. *Chemosphere* **2019**, *222*, 637−644.
(69) Ober, C. K.; Kafer, F.; Deng, J. Review of Essential Use of Fluorochemicals in Lithographic Patterning and Semiconductor Processing. *JM3* **2022**, *21* (1), No. 010901.
(70) Aravindan, V.; Gnanaraj, J.; Madhavi, S.; Liu, H.-K. Lithium-Ion Conducting Electrolyte Salts for Lithium Batteries. *Chemistry—A European Journal* **2011**, *17* (51), 14326−14346.
(71) Jackson, D. A.; Young, C. J.; Hurley, M. D.; Wallington, T. J.; Mabury, S. A. Atmospheric Degradation of Perfluoro-2-Methyl-3-Pentanone: Photolysis, Hydrolysis and Hydration. *Environ. Sci. Technol.* **2011**, *45* (19), 8030−8036.
(72) Burkholder, J. B.; Cox, R. A.; Ravishankara, A. R. Atmospheric Degradation of Ozone Depleting Substances, Their Substitutes, and Related Species. *Chem. Rev.* **2015**, *115* (10), 3704−3759.
(73) Ellis, D. A.; Mabury, S. A.; Martin, J. W.; Muir, D. C. G. Thermolysis of Fluoropolymers as a Potential Source of Halogenated Organic Acids in the Environment. *Nature* **2001**, *412* (6844), 321−324.

(74) Guelfo, J. L.; Ferguson, P. L.; Beck, J.; Chernick, M.; Doria-Manzur, A.; Faught, P. W.; Flug, T.; Gray, E. P.; Jayasundara, N.; Knappe, D. R. U.; Joyce, A. S.; Meng, P.; Shojaei, M. Lithium-Ion Battery Components Are at the Nexus of Sustainable Energy and Environmental Release of per- and Polyfluoroalkyl Substances. *Nat. Commun.* **2024**, *15* (1), 5548.
(75) Han, B.-C.; Liu, J.-S.; Bizimana, A.; Zhang, B.-X.; Kateryna, S.; Zhao, Z.; Yu, L.-P.; Shen, Z.-Z.; Meng, X.-Z. Identifying Priority PBT-like Compounds from Emerging PFAS by Nontargeted Analysis and Machine Learning Models. *Environ. Pollut.* **2023**, *338*, No. 122663.
(76) Li, J.; He, J.; Niu, Z.; Zhang, Y. Legacy Per- and Polyfluoroalkyl Substances (PFASs) and Alternatives (Short-Chain Analogues, F-53B, GenX and FC-98) in Residential Soils of China: Present Implications of Replacing Legacy PFASs. *Environ. Int.* **2020**, *135*, No. 105419.
(77) Chang, W.; Xu, S.-D.; Liu, T.; Wu, L.-L.; Liu, S.-T.; Liu, G.; Sun, J.; Luo, Y.-X.; Gao, L.; Li, H.; Lu, Q.; Yuan, Z.; Liu, K.-Y.; Zhou, H.; Zhang, X.-D.; Huang, Y.-C.; Xiong, Y.-W.; Zhu, H.-L.; Xu, D.-X.; Wang, H. Risk Prioritization and Experimental Validation of Per- and Polyfluoroalkyl Substances (PFAS) in Chaohu Lake: Based on Nontarget and Target Analyses. *J. Hazard. Mater.* **2025**, *492*, No. 138179.

https://doi.org/10.1021/acs.est.5c09274
Environ. Sci. Technol. 2025, 59, 25138−25150